Hyperfine-structure study of the $3d^{10}5p\ ^2P_{3/2}$ level of neutral copper using pulsed level-crossing spectroscopy at short laser wavelengths

J. Bengtsson, J. Larsson, S. Svanberg, and C.-G. Wahlström
Department of Physics, Lund Institute of Technology, P.O. Box 118, S-221 00 Lund, Sweden
(Received 24 May 1989)

A hyperfine-structure study of the strongly perturbed $3d^{10}5p\ ^2P_{3/2}$ state of neutral copper was performed using pulsed level-crossing spectroscopy. Excitation was accomplished at the short wavelength of 202 nm, where intense laser pulses were obtained using frequency tripling of dye laser radiation. For ^{63}Cu we obtained $a=61.7(9)$ MHz, $b=4.9(7)$ MHz, and $\tau=25,5(10)$ ns for the magnetic dipole and the electric quadrupoles interaction constants and the lifetime, respectively. A comparison with theoretical calculations based on the multiconfiguration Hartree-Fock method is made. A discussion of the usefulness of level-crossing, quantum-beat, and radio-frequency techniques for high-resolution spectroscopy at wavelengths in the uv and vacuum-uv region is presented.

I. INTRODUCTION

The copper atom has a $4s\ ^2S_{1/2}$ ground state, as has the potassium atom, but because of the easily perturbed $3d^{10}$ subshell the energy-level system of copper is much more complicated than that of potassium. A partial energy-level diagram for copper is given in Fig. 1. Levels belonging to the $3d^9 4s 4p$ configuration strongly perturb the alkali-atom-like doublet spectrum,[1] leading to anomalous lifetime values in the *ns* and *nd* Rydberg sequences.[2] The fine structures in the *np* sequence are extremely perturbed[3] and so are the lifetimes,[1] and this ^2P series was once quoted to be "probably the most distorted series known."[4]

Clearly, hyperfine-structure studies in this sequence are of considerable interest. In 1966 Ney reported data from an accurate level-crossing investigation of the $4p\ ^2P_{3/2}$ level, which was excited by a hollow-cathode lamp.[5] The $4p$ doublet could then later also be studied by high-resolution laser spectroscopy using single-mode laser excitation.[6–9] A many-body perturbation-theory calculation of the hyperfine structure of this doublet has been performed, but agreement with the experimental results was poor.[10] The next higher state, $5p\ ^2P$, exhibits a fine structure of only 9 GHz, while the next few higher ^2P states have much larger splittings. A cw laser investigation of the $4p$ and $5p\ ^2P$ states, excited from the metastable $3d^9 4s^2\ ^2D$ states, populated in a collimated atomic beam emerging from a dc discharge has been performed by our group.[8,9] However, the hyperfine structure (hfs) of the $5p\ ^2P_{3/2}$ level could not be resolved due to residual Doppler broadening. Because of the considerable interest in the hyperfine structure in the $5p\ ^2P$ state we have performed a rather elaborate level-crossing experiment which provided the necessary spectroscopic resolution. A theoretical study of the hyperfine-structure behavior in this perturbed series has also been performed, yielding insight into the configuration-interaction perturbations.

The $5p\ ^2P_{3/2}$ level is situated 49 383 cm^{-1} above the ground state corresponding to an excitation line at 202.4

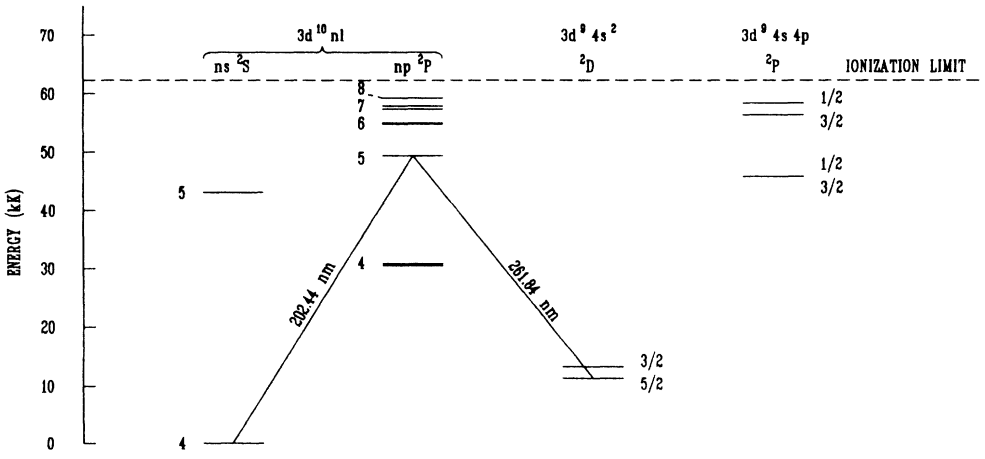

FIG. 1. Partial energy-level diagram for the copper atom.

nm. Single-mode dye laser radiation for high-resolution laser spectroscopy at such a wavelength cannot easily be obtained, although μW-range powers have been generated for the cooling of Hg^+ ions using 194-nm radiation.[11] Transitions from the metastable ^2D states at 262 and 277 nm can be induced with some effort, but it has not been possible to achieve a sufficiently large metastable population to allow for a strong reduction in the spectroscopic linewidth.[8,9] The quantum-beat method[12,13] would, in principle, be possible, but the hyperfine structure is too large to be tractable with the time resolution obtained from standard pulsed lasers, photomultiplier tubes, and transient digitizers. High-frequency quantum beats (up to 1 GHz) were recently observed for the $4p\ ^2P_{3/2}$ state, excited with the yellow line from the metastable state using a cw mode-locked laser system and photon counting techniques.[14] However, for a corresponding excitation of the $5p$ state a frequency-doubled laser is needed and the weak photon yield drowns in the discharge emission. In this situation the level-crossing (LC) method,[15] adopted for pulsed excitation and detection, provides a solution. The resolution of this technique is limited only by the Heisenberg uncertainty principle and not by the spectral and temporal characteristics of the laser source. In the same way as this method could once open up a whole new domain of hyperfine-structure studies when combined with broadband tunable lasers at visible wavelengths,[16–18] it can in its pulsed version extend precision investigations to the short uv and vacuum-uv (vuv) region, where only pulsed laser radiation can be readily obtained using nonlinear optical techniques. This is illustrated by the present work, performed with broadband excitation at 202 nm.

In Sec. II a theoretical background to the level-crossing technique is given. The experimental setup used is described in Sec. III, followed by a presentation of the measurements and results in Sec. IV. A theoretical discussion of the hyperfine structure in the lower ^2P states of copper can be found in Sec. V. Finally, a discussion of possibilities of high-resolution studies at short uv and vuv wavelengths is presented.

II. EXPERIMENTAL METHOD

The theory of resonance scattering of light by atoms was developed by Breit[19] in 1933 and popularized by Franken[20] in 1961. The total intensity of scattered light with polarization vector **g** following excitation by light with another polarization vector **f** was derived in both the above-mentioned papers. According to the Breit formula the scattered intensity is given by

$$S = C \sum_{\substack{m,m' \\ \mu,\mu'}} \frac{f_{\mu m} f_{m\mu'} g_{m'\mu} g_{\mu' m'}}{\frac{1}{\tau} + \frac{i}{\hbar}(E_\mu - E_{\mu'})} .$$

The symbols $f_{\mu m}$ denote matrix elements of the type $\langle \mu | \mathbf{f} \cdot \mathbf{r} | m \rangle$ where μ and m refer to wave functions for substates of an excited state and a ground state, respectively. The lifetime of the excited state is τ and the total energy of a substate is E_μ. The summation is performed over all ground and excited substates.

From the Breit formula it follows that when two levels intersect, the denominator becomes resonant and a change in the intensity of the scattered light can be detected. When the detection and excitation polarizations are perpendicular to the magnetic field such resonances can be experimentally seen only for intersecting levels whose magnetic quantum numbers differ by two units, as the fourfold product in the numerator is then nonzero. This is due to the fact that both states must be coherently excited by the same (σ) photon.

When performing a LC experiment, an external magnetic field is applied, the magnetic sublevels are scanned, and the scattered light intensity is recorded as a function of the varying magnetic field. An energy-level diagram for the $5p\ ^2P_{3/2}$ state of ^{63}Cu is given in Fig. 2. There are two stable isotopes of copper. Both have the nuclear spin $I = \frac{3}{2}$. The abundances of the isotopes are 69% for ^{63}Cu and 31% for ^{65}Cu. As can be seen from Fig. 2, in zero magnetic field, all magnetic sublevels of a hyperfine component have the same energy. A large zero-field or Hanle signal can thus be seen.[21] As shown in Fig. 2, four $\Delta\mu = 2$ crossings occur in intermediate fields. The fourth of these is generally difficult to observe experimentally. The positions of the crossings fully determine both the magnetic dipole and electric quadrupole interaction constants, normalized to the g_J factor.

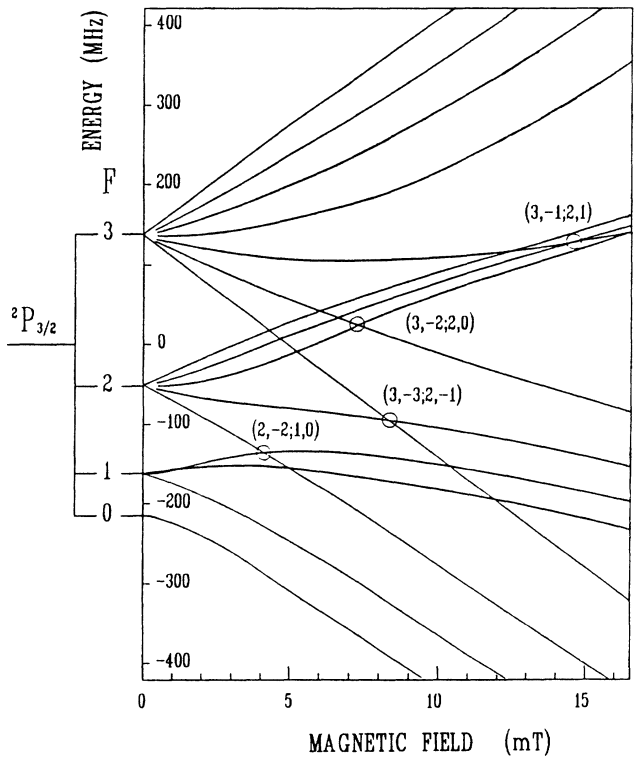

FIG. 2. Magnetic field dependence of the magnetic hyperfine substates for the $5p\ ^2P_{3/2}$ state of ^{63}Cu. $\Delta\mu = 2$ crossings are indicated using the symbol $(F,\mu;F',\mu')$.

Apart from the rapidly varying resonances another effect is present. As the magnetic field is varied, the matrix elements in the numerator of the Breit formula are changed from their Zeeman to their Paschen-Back values. The decoupling-dependent scattering is known as the Heydenburg effect.[22,23] The Heydenberg effect is manifested as a little structured slope in the scattering intensity as a function of the magnetic field. As can be seen from the above discussion, the information from such a magnetic field scan is rather complex, and a computer code that is able to simulate the scan is very useful for the interpretation.

The resolution in hfs measurements using the LC method is limited only by the Heisenberg uncertainty relation, and the width of the crossings is proportional to $1/\tau$. Individual crossings or the Hanle signal can thus be used to determine the lifetime of excited states.

It has been theoretically[24] and experimentally[25] proved that coherence signals such as the Hanle signal or optical double resonance[26] (ODR) signals are narrowed at high atomic density. This effect is called coherence narrowing. If all the scattering atoms experience the same magnetic field, the information about the phase of a decaying state and the orientation of the atom can be transferred from one atom to another by a photon. This makes it possible for the light to keep its coherence longer than the excited-state lifetime. Hence, in lifetime measurements using the Hanle method, extrapolation to zero atomic density must be performed to find the correct lifetime.

The Breit formula is derived based on the assumptions of broadband excitation and that all the scattered light in the temporal domain contributes to the signal. The effects of narrow-band excitation have been investigated by Series, Cohen-Tannoudji, and others.[27–29] When the exciting laser light partially resolves the hfs of the ground or excited state a weighting of the hfs levels occurs. The width of the individual Hanle effect contributions is proportional to $1/g_F$, and thus the width of the resulting Hanle signal will depend on where in the excitation profile the laser is tuned. This may be a complication if a lifetime determination is to be performed.[30] Narrow-band excitation can also be used to enhance individual crossings and thereby improve the signal-to-noise ratio.[31]

When detection is not initiated directly following the excitation, but after a certain delay, the LC resonances are narrowed and the shape of the resonances becomes more complex. Such delayed detection can be used to achieve subnatural linewidths.[32–34,31]

When using the LC method, all the experimentally determined parameters are in units of the Landé (g_J) factor. This factor can, in most cases, be determined either experimentally by optical Zeeman spectroscopy or ODR spectroscopy or can be theoretically calculated with high accuracy.

III. EXPERIMENTAL SETUP

The experimental setup is illustrated in Fig. 3. The laser system used was a Quantal Datachrome 5000. It consists of a YG 581c Q-switched Nd:YAG laser (YAG denotes the yttrium aluminum garnet) and a TDL 50 dye laser, which was operated on a mixture of Rhodamine 640 and Rhodamine 610 in methanol. In order to obtain the short excitation wavelength at 202.4 nm the dye laser output at 607.2 nm was frequency doubled in a potassium dihydrogen phosphate (KDP) crystal and the second harmonic and fundamental frequency outputs from the dye laser were mixed in a β-barium borate (BBO) crystal. This procedure of second-harmonic generation and subsequent mixing of the fundamental and second-harmonic frequencies results in a tripling of the fundamental frequency. This is a relatively new method of generating high-power laser pulses down to about 197 nm.[35] With this procedure, we could obtain an energy of approximately 2 mJ per pulse at 202 nm when using 70 mJ per pulse at 607 nm.

The free copper atoms were produced as a beam from an oven in a vacuum system. Two pairs of Helmholtz coils produced a magnetic field. The polarization of the laser beam was chosen to be orthogonal to the magnetic field in order to induce σ transitions. Detection of the fluorescence light from the atomic beam was performed in two directions. One of these was orthogonal to the incident laser beam and parallel to the magnetic field. In this direction, only σ photons can be detected. The other direction was at 135° relative to the incident laser beam and orthogonal to the magnetic field. In this direction both σ and π photons can be detected. The photons were detected using EMI 9558 QA photomultiplier tubes through interference filters and linear polarizing filters. In the 135° direction the linear polarizer was oriented for σ detection. When using σ detection in this direction the Hanle and level-crossing signals will have a dispersion line shape. The detected signal in the magnetic field direction can be chosen to be dispersive with the opposite sign. This is achieved by orienting the polarizer 45° relative to the polarization of the incident laser radiation. The ratio of these two signals will also be dispersion shaped, provided that the signal is much smaller than the incoherent fluorescence intensity. Thus the coherent-signal–to–incoherent-background ratio is increased by a factor of 2.

The intensity fluctuations of pulsed lasers due to pulse-to-pulse variations are normally of the order of 10%. This can be a problem when detecting signals smaller than these fluctuations. One way to compensate for these pulse-to-pulse variations is to monitor the laser intensity on a linear diode and normalize the detected signal. A better way, as explained above, is to use two fluorescent light detectors and divide the two signals. This will double the signal amplitude and normalize the fluorescence intensity, which effectively takes care of the intensity fluctuations. The fact that normal photomultiplier tubes are slightly nonlinear will cause two detectors that are not perfectly matched to respond slightly differently to intensity fluctuations and the normalization will not be perfect. In order to compensate for this differential nonlinearity we used a scheme proposed by Wolf and Tiemann.[36] The idea is to record this differential nonlinearity and compensate for it. One way to do this is to leave the experiment on standby and let both detectors measure the fluorescence signal from the

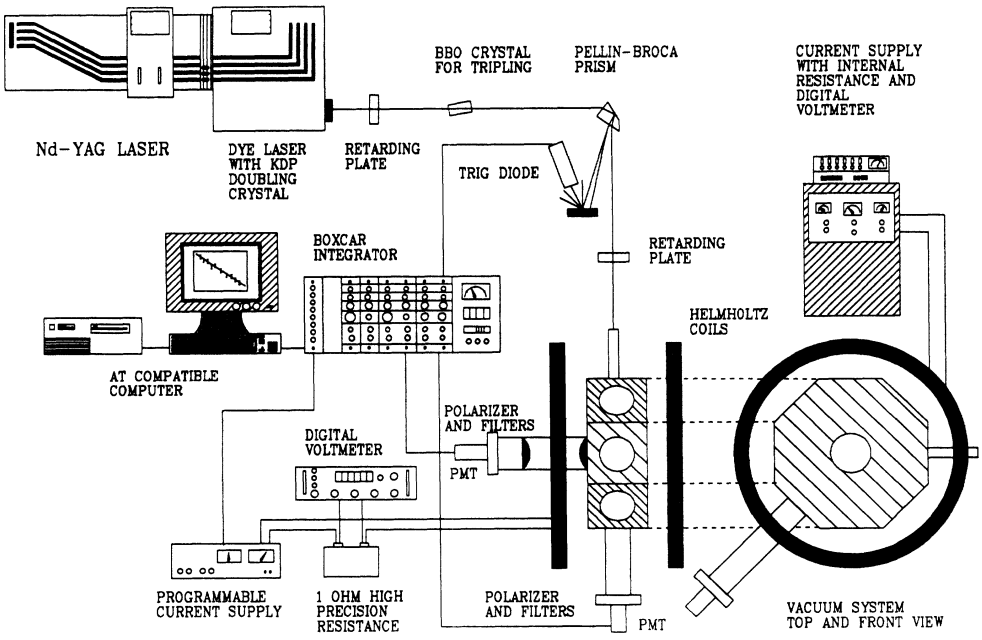

FIG. 3. Experimental setup. PMT denotes photomultiplier tube and BBO β-barium borate.

same sequence of laser pulses. The response from one detector is plotted against the response from the other, and a polynomial, for example, is fitted to this sequence of measured points. This polynomial can be considered as a calibration curve which gives the signal from one detector as it would have been if measured by the other. When performing the actual experiment, the signal from one detector and the recalculated signal from the other, will have the same response to intensity fluctuations.

A Stanford Research SR 265 boxcar integrator was used to process the detected fluorescence. This was connected to an IBM-compatible AT computer. The computer code provided with the SR 265 unit was extended to include the above-mentioned features. The signal from each channel was transferred from the boxcar to the computer directly for each laser pulse and the calculations were performed on line with the experiment. The temporal gates on the boxcar integrator were set so as to be long enough to record the whole fluorescence signal.

The magnetic sweep field was generated by a Hewlett Packard HP6267B dc power supply which was controlled by a ramp voltage. This ramp was generated by the computer using a digital-to-analog converter in the boxcar unit. Normally, the sweep current was connected to the smaller of two sets of coaxial Helmholtz coils. The current was monitored using a 1-Ω high-precision resistor in series with the coils. The other set of coils was used to produce a static magnetic field. This set was supported by a Bruker power supply, which is a highly stabilized current generator with an internal resistor for current measurement.

Calibration of the magnetic field and compensation of the vertical component of the Earth's magnetic field were performed using optical pumping of a ^{133}Cs cell. From observed rf resonances a calibration accuracy of 2 parts in 10^4 was achieved.

For some of the recordings a faster detection system was needed. A g_J-independent lifetime measurement and recordings of fast Zeeman quantum beats were performed using a Hamamatsu 1564U microchannel plate photomultiplier tube.

IV. MEASUREMENTS

A. Theoretical considerations

After populating the $5p\ ^2P_{3/2}$ state from the $4s\ ^2S_{1/2}$ ground state, it would be advantageous to detect fluorescence down to a $J=1/2$ state in order to achieve a maximum signal-to-incoherent-background ratio. Theoretically, the Hanle signal in such a case will be about 20% of the total scattered light. The transition back to the ground state was observed to be weaker than the transitions down to the metastable $3d^9 4s^2\ ^2D_{3/2,5/2}$ states. This fact, combined with the technical problems of finding high-efficiency polarizers and interference filters at a wavelength of 202 nm, meant that this detection scheme was not feasible. As it was not possible to separate the two $5p\ ^2P$ states in excitation, due to the small fine structure, the transition with the metastable $^2D_{5/2}$ state was used for detection in order to suppress the $^2P_{1/2}$-level decay to the selection rule. Also, the $J=3/2\rightarrow J=5/2$ transition is much stronger than the $J=3/2\rightarrow J=3/2$ transition. The experimental Hanle signal was found to be about 3% of the total intensity of the scattered light. The intermediate-field crossings were about 0.2–0.5 % for the dominating ^{63}Cu isotope.

The normalization algorithm described in Sec. III

effectively eliminated pulse-to-pulse fluctuations, and the noise level was determined by photon statistics. In order to achieve a maximum signal-to-noise ratio the atomic density was normally kept rather high, and a large coherence narrowing was observed. This, in fact, increased the resolution in the spectra. At still higher atomic densities the coherence was reduced due to collisions. This resulted in a reduction in the signal amplitude and a broadening of the signal. As the detection directions were not geometrically equivalent, different coherence times (effective lifetimes) could be expected in the two directions. A small deviation of the experimental signal, obtained as the quotient of the signal in the two directions, from the theoretical signal which occurred only at high atomic densities implies that such was the case.

The laser that was used is narrow banded enough to partially resolve the hfs in the ground state (about 12 GHz). The excitation can therefore not be considered to be broadband, since the population distribution of the excited hyperfine states is changed if the laser is scanned through the excitation profile, due to the transition rules. This hyperfine weighting was used to enhance the individual crossings, as first demonstrated in Cs experiments.[31]

B. Experimental recordings

In order to determine the hfs of a state, the high-field signals must be located. This can invoke a tedious search, especially for weak signals, as in our case. If the hfs is very small, and unmeasurable, all crossings collapse into the Hanle signal, since the Paschen-Back region of the hfs is reached already in the field region of the Hanle effect. The Hanle signal then corresponds to one in a pure fine-structure state, and the width of the signal is proportional to $1/g_J\tau$. If, on the other hand, the hfs is large, the Hanle effect is composed of a number of dispersion shaped contributions from the individual F levels. These contributions will have widths proportional to $1/g_F\tau$ and intensities that depend on the spectral weighting, in the case of narrow-band excitation.[30] However, the situation is much simplified in our case, since $I=J$ and thus $g_F=\frac{1}{2}g_J$ for all F levels. Thus the shape of the Hanle signal, in a large hfs case, is described by a dispersion curve and the width is proportional to $1/(\frac{1}{2}g_J\tau)$. Since the lifetime of the studied state has been independently determined to be 23(2) ns,[2] a measurement of the halfwidth of the Hanle signal should distinguish between the cases of a very small and a large hfs. However, computer simulations with the Breit formula reveal that an almost dispersion-shaped signal, with a width corresponding to the large hfs case, would also be obtained for a small but non-negligible hfs ($a\simeq 3$ MHz), when the crossing signals are still not resolved, but influence the shape of the Hanle signal. Preliminary recordings indicated this undecided case. To distinguish between the two cases an independent measurement of the g factor was desirable. According to the discussion above, a Zeeman quantum-beat experiment for the large hfs case would yield a single beat frequency of $\nu=2g_F\mu_B B$ ($\Delta\mu=2$ signals), while a distribution of frequencies would be obtained for the intermediate hfs case and a single beat frequency at double the frequency, 2ν, for the pure fine-structure (low hfs) case.

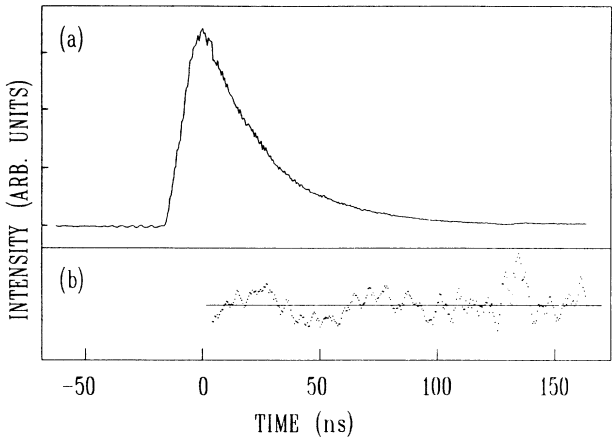

FIG. 4. (a) Recordings of the time-resolved fluorescence from the $5p\ ^2P_{3/2}$ state in Cu and (b) Zeeman quantum beats recorded at a magnetic field of 0.982 mT using the fast detector setup.

Experimental Zeeman quantum-beat recordings were performed in a field region of 0.5–1.0 mT, where clear discrimination between the cases can be made. A single, faster photodetector was used in these measurements, in order to also allow a g_J-independent determination of the lifetime. In Fig. 4(a), such a time-resolved recording is shown. Because of the unfavorable J-value sequence in the excitation-detection scheme, the beats have a very small amplitude, but can be made visible, as shown in Fig. 4(b), by dividing two recordings, detected through perpendicularly oriented polarizers, to achieve a maximum enhancement of the beats. For a magnetic field of 0.98 mT, a beat frequency of 19(1) MHz was found, corresponding to $g=\frac{1}{2}g_J$ and a large hfs. Thus there will be

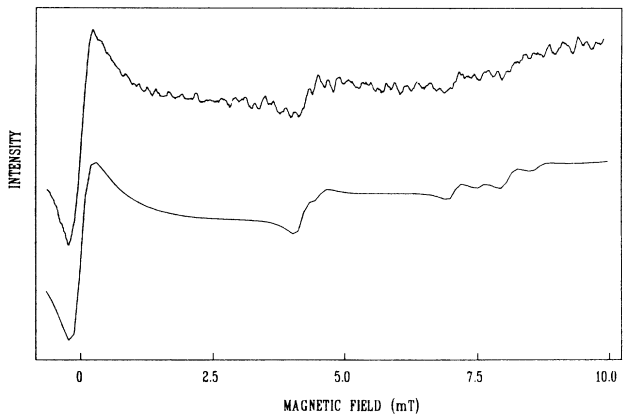

FIG. 5. A magnetic field scan over a large interval showing the magnetic field dependence of the fluorescence light with the zero-field Hanle effect and high-field crossing signals for the $5p\ ^2P_{3/2}$ state. A theoretical curve obtained from a computer calculation with the final fitted parameters is included.

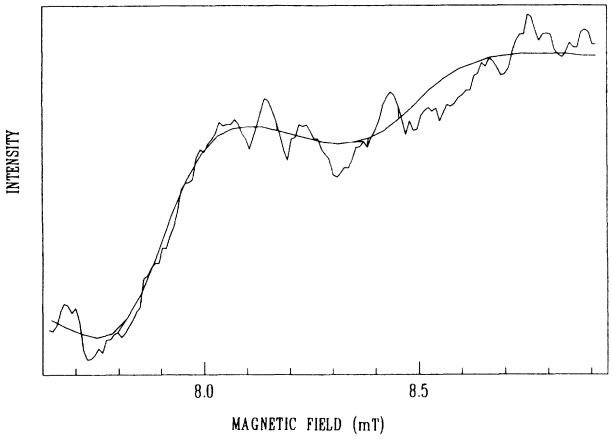

FIG. 6. Experimental recording of the third crossing of the two copper isotopes and a theoretical curve calculated from the Breit formula. In the calculation the final hyperfine parameters were used and an effective lifetime of 38 ns.

separated high-field level-crossing signals and a search is warranted. In scans covering the field region 0–11 mT the expected crossings were actually found. An overview recording is shown in Fig. 5. Eight hours of data collection were required to obtain this curve, since the signals constitute such a low fraction of the total light. In order to obtain accurate determinations of the crossing positions, scans were performed in small field regions at the crossings. Such a scan, together with a theoretical curve derived from the Breit formula, is shown in Fig. 6. For the theoretical curve, the effective lifetime and detection polarization determined from a Hanle curve with good signal-to-noise ratio were used. In order to determine the atomic lifetime of the $5p\ ^2P_{3/2}$ state by the Hanle method, several Hanle signals for different atomic densities were recorded.

C. Evaluation

In the recordings the signals from the two isotopes are superimposed. However, the ratios between the hyperfine constants are known from other methods. A higher overall accuracy in the evaluation can be obtained by fitting just two hyperfine-structure parameters to the structures. The ratio of the nuclear magnetic moments and hence the magnetic dipole interaction constants (neglecting the hfs anomaly) has been determined from nuclear magnetic resonance to be $\mu_I(^{65}\mathrm{Cu})/\mu_I(^{63}\mathrm{Cu}) = 1.071\,27(2)$.[37] The ratio of the electrical quadrupole moments $Q(63)/Q(65) = 1.0806(3)$ has been measured by the nuclear quadrupole resonance method.[38] With these ratios known, experimental a and b factors for the $5\ ^2P_{3/2}$ state are given for the dominant ^{63}Cu isotope only. The positions of the crossings for the ^{63}Cu isotope were determined and these magnetic fields are given below:

$$C_1 = 4.32(2)\ \mathrm{mT},\quad C_2 = 7.24(3)\ \mathrm{mT},\quad C_3 = 8.39(2)\ \mathrm{mT}\ .$$

The positions of the crossings give the hyperfine structure parameters

$$a(5\ ^2P_{3/2};^{63}\mathrm{Cu}) = 61.7(9)\ \mathrm{MHz}\ ,$$

$$b(5\ ^2P_{3/2};^{63}\mathrm{Cu}) = 4.9(7)\ \mathrm{MHz}\ .$$

As previously mentioned, all results obtained by the level-crossing method are normalized to the g_J factor. As no accurate experimental value was available and a precision measurement with pulsed ODR was deemed difficult because of the short lifetime of the state, we have used a theoretical g_J value of 1.334 as calculated using the mixing coefficients given by Carlsson.[1] The uncertainty in this value should be less than a few parts per thousand and does not influence the final accuracy of the hfs interaction constants. Only the relative signs of the a and b factors are given in a LC experiment. However,

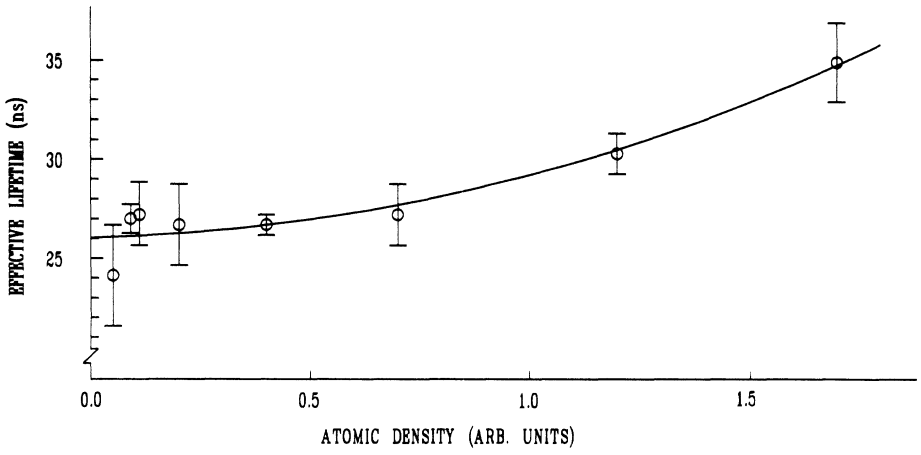

FIG. 7. The effective lifetimes corresponding to the width of the measured Hanle resonances plotted vs the atomic density. Extrapolation to zero atomic density gives the lifetime.

the sign of the a factor is known to be positive from the recent single-mode laser experiments.[9]

The error bars given for the hfs parameters reflect the fact that a fully consistent evaluation of the a and b parameters is not obtained when using different combinations of the three crossings. The discrepancy corresponds to about 15% of a full crossing linewidth. The perturbations are mainly due to second-order hfs effects induced by the presence of the other fine-structure component $5p\ ^2P_{1/2}$, only 9 GHz above the $5p\ ^2P_{3/2}$ level. Knowledge of the off-diagonal hyperfine interaction constants is needed to perform an accurate correction. Since we could thus not apply a second-order hfs correction, the error bars for a and b are larger than otherwise motivated from statistical signal errors.

In order to evaluate the lifetime of the state, the effective lifetime, as given by the width of the Hanle signal at different atomic densities, is plotted in Fig. 7. Extrapolation to zero atomic density yields the lifetime

$$\tau(5p\ ^2P_{3/2})=26.0(15)\ \text{ns}\ .$$

From time-resolved measurements using the fast detector setup, the lifetime obtained is

$$\tau(5\ ^2P_{3/2})=25.2(10)\ \text{ns}\ .$$

The above value was obtained as the average of a large number of measurements at low atomic densities and the error given corresponds to two standard deviations. A weighted mean value of these two measurements is

$$\tau(5\ ^2P_{3/2})=25.5(10)\ \text{ns}\ .$$

This value is consistent with our previously reported value 23(2) ns although more accurate.[2]

V. THEORETICAL INTERPRETATION

As pointed out in the Introduction, the $3d^{10}np\ ^2P$ series in Cu is strongly perturbed. The fine structures and the radiative lifetimes observed deviate drastically from predictions based on central field models, such as single-configuration Hartree-Fock (HF). Making a comparison between the HF values for the magnetic dipole interaction constants and the corresponding experimental values, Table I, clearly shows that the hyperfine interactions are also severely perturbed.

The irregular trends in the fine structures and the radiative lifetimes in the $np\ ^2P$ series were studied by Carlsson[1] with the multiconfiguration Hartree-Fock method, including relativistic effects to first order. The most dominant perturbations were found to be due to the interaction between members of the $3d^{10}np$ Rydberg series and different states belonging to the doubly excited configuration $3d^9 4s4p$. In a strict *ab initio* calculation, using the set of configurations chosen by Carlsson, levels of the $3d^9 4s4p$ configuration are located some 5000–9000 cm^{-1} too high relative to the Rydberg series, resulting in completely erroneous mixing coefficients. (This indicates one of the reasons why an *ab initio* perturbation calculation, as in Ref. 10, must be taken to very high orders to account for this mixing correctly.) To circumvent this problem, Carlsson manually corrected the average energies of the $3d^9 4s4p$ terms before diagonalization. Using the eigenvectors and eigenvalues obtained in this way, good agreement was found between calculated and observed fine structures and radiative lifetimes.

It is outside the scope of the present work to perform a complete hyperfine calculation, but we would like to show that the admixtures of the $3d^9 4s4p$ configuration give important contributions to the observed large dipole interaction constants. To do so we will use the eigenvectors obtained by Carlsson.[1,39]

The radial eigenfunctions used are nonrelativistic, but since relativistic effects are included to first order in the energy matrix before diagonalization, important relativistic effects are still incorporated. One important example of this is the J-dependent mixing coefficients used. The $3d^9 4s4p$ configuration gives rise to nine different terms. Two of these are ^2P terms, one with an energy lower than the $3d^{10}5p\ ^2P$ term investigated in the present work, and one with higher energy. The fine-structure splitting of the high-lying ^2P term is large, about 2000 cm^{-1}, and the structure is inverted, while the corresponding splitting of the $3d^{10}5p\ ^2P$ term is extremely small, only about 0.3 cm^{-1}. The energy difference between the $J=1/2$ states is therefore about 2000 cm^{-1} larger than the corresponding energy difference for the $J=3/2$ states, and consequently there are different amounts of $3d^9 4s4p$ character in the two states of the $5p\ ^2P$ term. We can therefore apply a nonrelativistic hyperfine operator to one state at a time and account for these relativistic, J-dependent, effects.

The magnetic dipole interactions are represented, in a nonrelativistic treatment, by the operator[40]

$$h_d=\alpha^2\sum_{i=1}^{N}\left[\mathbf{l}r^{-3}-\sqrt{10}(\mathbf{sC}^2)^1 r^{-3}+\frac{8\pi}{3}\mathbf{s}\delta(\mathbf{r})\right]\cdot\boldsymbol{\mu}_I\ .$$

Here $\mathbf{l}$ and $\mathbf{s}$ are the orbital and spin angular momentum operators, respectively, of the ith electron, $(\mathbf{sC}^2)^1$ is a tensor product of $\mathbf{s}$ and $\mathbf{C}^2$ of rank 1 ($\mathbf{C}^2$ is a renormalized spherical harmonic), and $\delta(\mathbf{r})$ is a three-dimensional delta function. $\boldsymbol{\mu}_I$ is the nuclear magnetic moment.

The electronic part, given by the sum of the terms within the large parentheses, represents the magnetic field at the site of the nucleus due to the electrons. The first term is due to the orbital motion of the electrons, and is called the orbital term. The second term represents the dipole field due to the spin motion of the

TABLE I. Magnetic dipole interaction constants for ^{63}Cu in megahertz. References to the experimental values are given. Values in parentheses denote error bars.

	$3d^{10}4p\ ^2P$		$3d^{10}5p\ ^2P$	
	$J=1/2$	$J=3/2$	$J=1/2$	$J=3/2$
HF	278	55.5	79.5	15.9
Observed	507(10)[a]	194.72(15)[b]	335(37)[a]	61.7(9)[c]

[a]Reference 9.
[b]Reference 5.
[c]This work.

electrons and is called the spin-dipole term. These two terms, which have an r^{-3} radial dependence, contribute only for non-s electrons. The last term of the dipole operator represents the contact interaction between the nucleus and the electron spin, and contributes only for s electrons. The summation includes all electrons, but in a central field model there is no contribution from filled shells due to spherical symmetry.

When calculating energy shifts diagonal in **I** and **J**, or evaluating observed hyperfine structures, we usually replace the operator above by the equivalent operator

$$h_d = a\mathbf{I}\cdot\mathbf{J} ,$$

where a is the dipole interaction constant.

For each state of a given term, the a factor represents a certain linear combination of the orbital, spin-dipole, and contact interactions. With the experimental data available, and J-dependent eigenvectors, we cannot deduce experimental values of each of the three types of interaction. We are, therefore, in this work, limited to a comparison of theoretical and observed a factors.

When evaluating a factors from the eigenvectors[1,39] the important contributions to the deviation from the HF values come from the $3d^9 4s(^{1,3}D)4p\ ^2P$ basis vectors. These basis vectors do not represent the two observed ^2P terms mentioned above. The observed terms are represented by linear combinations of these basis vectors. An alternative representation, with higher purity for the $3d^9 4s4p\ ^2P$ terms, is obtained by first coupling the $4s$ and $4p$ electrons to $^{1,3}P$ terms and adding these to the $3d^9\ ^2D$ term. The left-to-right coupling ($^{1,3}D$) is used in Ref. 1; we will therefore use this coupling.

In Table II nonrelativistic dipole-interaction matrix elements are presented for each of the two basis vectors and the off-diagonal element between them. The orbital interaction, being spin independent, is equal for both basis vectors and identically zero for the off-diagonal term. These rather large contributions are mainly due to the $3d$ hole, having an r^{-3} expectation value almost ten times larger than the corresponding value for the $4p$ electron. This interaction increases all the a factors, irrespective of J quantum number or sign for the mixing coefficients.

The spins of the $3d$ and $4s$ electrons are coupled to a singlet in the ^1D parent term, and there is consequently no spin-dipole contribution from the $3d$ electron. Only a very small spin-dipole contribution from the $4p$ electron is present for this basis vector. Due to the tensor structure of the spin-dipole operator, the interactions for the basis vectors with the ^3D parent term are also rather small, especially for the $J=3/2$ state.

The interaction most critically reflecting the eigenvector compositions is obviously the Fermi contact term for the unpaired $4s$ electron. It contributes for $J=1/2$ and $J=3/2$ with equal magnitudes but with opposite signs. The off-diagonal matrix element is further dependent on the relative signs of the mixing coefficients in the total eigenvectors.

The interaction matrix elements for the basis vectors are much larger than the central field values for the $3d^{10}np$ configurations. Even small admixtures of $3d^9 4s4p$ therefore give large contributions to the a factors for the $3d^{10}np\ ^2P$ states. The mixing coefficients for the $3d^9 4s(^{1,3}D)4p\ ^2P$ states are given in Table III.

The admixture of these basis vectors is clearly different in the $4p$ and $5p$ eigenvectors. The ^1D basis vector dominates in the eigenvector for the $3d^{10}5p$ configuration while ^3D basis vector dominates for the $3d^{10}4p$ configuration. This gives rise to large orbital contributions for both configurations, but a much larger spin-dipole contribution for the $3d^{10}4p$ configuration, especially for the $J=3/2$ state. The diagonal contribution from the contact interaction (nonzero only for the ^3D parent) is more than an order of magnitude larger for the $4p$ than the $5p$ eigenvectors. In the $4p$ eigenvector the off-diagonal contribution, due to different signs for the basis vectors, is negative and cancels more than one-third of the diagonal contribution, while in the $5p$ eigenvectors these contributions add constructively. The total contact contributions to the a factors for these two $3d^{10}np$ configurations are therefore, with the mixing coefficients we have used, approximately equal.

Adding the different contributions from the $3d^9 4s4p$ configuration to the Hartree-Fock values, considerable improvements are obtained for the $3d^{10}4p$ states. The a factors increase from 278 to 450 MHz for the $J=1/2$ state and from 56 to 168 MHz for the $J=3/2$ state. These values should be compared with the experimental values of 507 and 194 MHz, respectively. The improvement for the $5p\ ^2P_{1/2}$ state is, relatively speaking, even better, from 79.5 to 173 MHz. But the experimental value is 335 MHz, so there is still 148 MHz missing. For the $5p\ ^2P_{3/2}$ state the a factor increases from 15.9 to 161 MHz. This is about 100 MHz larger than the experimental value of 61.7 MHz obtained in the present work.

When examining this comparison, one should bear in mind, however, that the off-diagonal contact interactions, for example, give contributions critically dependent on the mixing coefficients. A different sign, for example, of the very small ($\leq 0.4\%$) mixing coefficient for the $3d^9 4s(^3D)4p$ basis vector would increase the a factor for the $J=1/2$ state by about 60 MHz and decrease the a

TABLE II. Basis vector dipole interaction matrix elements (in gigahertz) for ^{63}Cu.

	Orbital		Spin-dipole		Contact	
$3d^9 4s(^{1,3}D)4p\ ^2P_J$	$J=1/2$	$J=3/2$	$J=1/2$	$J=3/2$	$J=1/2$	$J=3/2$
$^1D,^1D$	+2.2	+1.1	0.02	−0.002		
$^3D,^3D$	+2.2	+1.1	0.5	−0.05	−1.6	+1.6
$^1D,^3D$			−0.5	+0.05	−1.4	+1.4

TABLE III. Mixing coefficients for the $3d^9 4s(^{1,3}D)4p\ ^2P$ basis vectors in the $3d^{10}np\ ^2P$ eigenvectors. The coefficients squared are given in parentheses (from Ref. 1).

Basis vector	$4p$ $^2P_{1/2}$	$4p$ $^2P_{3/2}$	$5p$ $^2P_{1/2}$	$5p$ $^2P_{3/2}$
^1D	−0.055 (0.3%)	−0.045 (0.2%)	+0.232 (5.4%)	+0.268 (7.2%)
^3D	+0.207 (4.3%)	+0.215 (4.6%)	+0.044 (0.2%)	+0.066 (0.4%)

factor for the $J=3/2$ state by about 100 MHz.

It is clear from the above discussion that the interaction between the $3d^{10}np$ Rydberg series and the $3d^9 4s4p$ configuration is of major importance for the understanding of the large experimental a factors. It should likewise be clear that quantitative calculations of the contributions to the a factors from these configuration interactions require extremely accurate mixing coefficients, as regards magnitudes as well as relative signs. The experimental hyperfine structures reported on in this work can therefore serve as sensitive tests for future theoretical calculations of wave functions.

VI. DISCUSSION OF HIGH-RESOLUTION SPECTROSCOPY AT SHORT uv AND vuv WAVELENGTHS

Several methods are available for the determination of atomic hyperfine structures,[41] including a variety of high-resolution laser spectroscopic techniques using cw single-mode dye lasers.[42] However, when short-uv excitation wavelengths are required, pulsed lasers are most easily used. Hfs measurements using pulsed lasers can be performed using quantum-beat spectroscopy[12,13] (QBS), optical double resonance[26] (ODR), or level-crossing spectroscopy[15] (LC).

QBS is an attractive method, when measuring hfs splittings of sizes compatible with the available temporal resolution of the pulsed laser, the photomuliplier and transient digitizer. The possibility of measuring the complete decay in fluorescence provides an efficient means of signal averaging. Furthermore, the interpretation of the signals is straightforward using Fourier-transform algorithms. Quantum-beat measurements at short wavelengths are possible up to a frequency of about 1 GHz but require very advanced equipment including a Q-switched and mode-locked laser system, fast microchannel photomultiplier tubes, and the fastest transient digitizers available.

In zero-field ODR the size of the hfs that can be studied is limited only by the magnetic rf or microwave field frequencies that can be produced. It is more common to apply ODR at intermediate or high magnetic fields. A special advantage of ODR is that signals can also be observed in states populated in cascades from higher-lying levels. When using pulsed excitation, high intensity pulsed rf fields can be applied to study even very short-lived states.

In LC, the size of the hfs to be studied is limited by the strength of the magnetic field that can be produced. Fields of the order of 1 T can be produced to study hyperfine and fine structures of the order of 10 GHz. Since no rf field is needed to induce transitions, this method is quite simple. Generally speaking, the level crossing method has an all-round applicability and puts the smallest demands on the experimental equipment used when performing high-resolution studies in "difficult" wavelength regions.

In this paper, we have drawn attention to the possibility of combining resonance methods with pulsed lasers for hyperfine-structure studies at short wavelengths. We have demonstrated the usefulness of tripling in BBO crystals for producing high-power laser radiation in the short uv region. This method combined with coherent anti-Stokes Raman scattering can be a powerful method for the production of tunable laser radiation in the upper vuv region. Studies of hfs in high-lying states of Cu and Ag and other atoms using such short-wavelength radiation are being planned to fully exploit the power of the experimental techniques described in this paper.

ACKNOWLEDGMENTS

This work was supported by the Swedish Natural Science Research Council.

[1] J. Carlsson, Phys. Rev. A **38**, 1702 (1988).
[2] J. Carlsson, A. Dönszelmann, H. Lundberg, A. Persson, L. Sturesson, and S. Svanberg, Z. Phys. D **6**, 125 (1987).
[3] C. Moore, *Atomic Energy Levels,* Natl. Bur. Stand. Ref. Data Ser. Natl. Bur. Stand. 35 (U.S. GPO, Washington, D.C., 1971), Vol. II.
[4] A. G. Shenston and H. N. Russel, Phys. Rev. **39**, 415 (1932).
[5] J. Ney, Z. Phys. **196**, 53 (1966).
[6] D. C. Gerstenberger, E. L. Latush, and G. S. Collins, Opt. Commun. **31**, 28 (1979).
[7] Ph. Dabkiewicz and T. W. Hänsch, Opt. Common. **38**, 351 (1981).
[8] H. Bergström, H. Lundberg, W. X. Peng, A. Persson, S. Svanberg, and C.-G. Wahlström, in *Resonance Ionization Spectroscopy 1986,* edited by G. S. Hurst and C. Grey Morgan (Institute of Physics, Bristol, 1987), p. 349.
[9] H. Bergström, W. X. Peng, and A. Persson, Z. Phys. D **13**, 203 (1989).
[10] J.-L. Heully, Z. Phys. A **319**, 253 (1984).
[11] H. Hemmati, J. C. Bergquist, and W. M. Itano, Opt. Lett. **8**, 73 (1983).
[12] J. N. Dodd and G. W. Series, in *Progress in Atomic Spectroscopy, Part A,* edited by W. Hanle and H. Kleinpoppen (Plenum, New York, 1978), p. 639.

[13]S. Haroche, in *High-Resolution Laser Spectroscopy,* Vol. 13 of *Topics in Applied Physics,* edited by K. Shimoda (Springer, Heidelberg, 1976), p. 253.
[14]J. Carlsson, L. Sturesson, and S. Svanberg, Z. Phys. D **11**, 287 (1989).
[15]F. D. Colgrove, P. A. Franken, R. R. Lewis, and R. H. Sands, Phys. Rev. Lett. **3**, 420 (1957).
[16]S. Svanberg, P. Tsekeris, and W. Happer, Phys. Rev. Lett. **30**, 817 (1973).
[17]S. Svanberg and P. Tsekeris, Phys. Rev. A **11**, 1125 (1975).
[18]S. Svanberg, in *Laser Spectroscopy III,* Vol. 7 of *Springer Series in Optical Sciences,* edited by J. L. Hall and J. L. Carlsten (Springer, Heidelberg, 1977), p. 187.
[19]G. Breit, Rev. Mod. Phys. **5**, 91 (1933).
[20]P. A. Franken, Phys. Rev. **121**, 508 (1961).
[21]W. Hanle, Z. Phys. **30**, 93 (1924).
[22]A. Ellet and N. P. Heydenburg, Phys. Rev. **46**, 583 (1934).
[23]N. P. Heydenburg, Phys. Rev. **46**, 802 (1934).
[24]J. P. Barrat, J. Phys. (Paris) **20**, 541 (1959); **20**, 633 (1959).
[25]J. P. Barrat, J. Phys. (Paris) **20**, 657 (1959).
[26]J. Brossel and F. Bitter, Phys. Rev. **86**, 368 (1952).
[27]G. W. Series, Proc. Phys. Soc., London **89**, 1017 (1966).
[28]D. Avan and C. Cohen-Tannoudji, J. Phys. (Paris) **36**, L85 (1975).
[29]C. Cohen-Tannoudji, in *Frontiers in Laser Spectroscopy, Vol. 1,* edited by R. Balian, S. Haroche, and S. Liberman (North-Holland, Amsterdam, 1972).
[30]S. Svanberg, Phys. Scr. **5**, 73 (1972).
[31]J. Larsson, L. Sturesson, and S. Svanberg, Phys. Scr. **40**, 165 (1989).
[32]H. Figger and H. Walther, Z. Phys. **267**, 1 (1974).
[33]J. S. Deech, P. Hannaford, and G. W. Series, J. Phys. B **7**, 1311 (1975).
[34]P. Schenk, R. C. Hilborn, and H. Metcalf, Phys. Rev. Lett. **31**, 189 (1973).
[35]W. L. Glab and J. P. Hessler, Appl. Opt. **26**, 3181 (1987).
[36]U. Wolf and E. Tiemann, Appl. Phys. B **39**, 35 (1986).
[37]H. E. Walchilli, Oak Ridge National Laboratory Report No. ORNL-1469, 1955, Suppl. II.
[38]H. Krüger and U. Mayer-Berkhout, Z. Phys. **132**, 171 (1952).
[39]J. Carlsson (private communication).
[40]I. Lindgren and J. Morrison, *Atomic Many Body Theory,* Vol. 13 of *Springer Series in Chemical Physics,* edited by J. P. Toennies (Springer, Heidelberg, 1982).
[41]S. Svanberg, *Atomic and Molecular Spectroscopy,* Vol. 6 of *Springer Series in Atoms and Plasmas,* edited by A. L. Schawlow (Springer, Heidelberg, in press).
[42]W. Demtröder, *Laser Spectroscopy,* Vol. 5 of *Springer Series in Chemical Physics,* edited by F. P. Schäfer (Springer, Heidelberg, 1988), 3rd corrected printing.